PERFORMANCE OF THERMAL INSULATION FABRICATED BY RAPID PROTOTYPING TECHNOLOGY

by

Maria TYCHANICZ-KWIECIEN*[*]*, Robert SMUSZ, and Pawel GIL

Faculty of Mechanical Engineering and Aeronautics,
Rzeszow University of Technology, Rzeszow, Poland

Original scientific paper
https://doi.org/10.2298/TSCI19S4079T

Nowadays, 3-D printing technology is very often applied in industry due to design cycles shortening and surface quality improvement when comparing to conventional manufacturing technologies. In order to adapt 3-D printed materials as thermal barriers, it is necessary to determine its thermophysical properties. As far as thermal insulation is concerned, the lowest thermal conductivity is required and therefore the crucial parameter of the material is the porosity. This paper presents the results of experimental investigation of effective thermal conductivity of thermal barriers with variable porosity fabricated by the fused filament fabrication technology. Also the numerical study was presented. The commercial code - COMSOL multiphysics was used to model the coupled heat transfer. The model was than validated by comparing the numerical and experimental results. For each sample the density and thermal conductivity were determined experimentally. The influence of the size and shape of the cell on the formation of free convection was investigated in particular. The effect of the conduction and radiation on temperature and velocity profiles within the enclosure has been analyzed. In addition, the dominant heat transfer mechanisms as a function of density have been identified.

Key words: *thermal insulation, rapid prototyping, heat transfer, thermal barrier, thermal conductivity*

Introduction

The 3-D printing technologies have great potential nowadays. It allows the fabrication of various components, especially of complex shape. Rapid prototyping (RP) methods, also known as additive manufacturing (AM) technologies, have been known for about 30 years and are currently competitive to traditional manufacturing processes to a certain extent. According to the ASTM Standard [1], AM is the process of joining materials to make objects from 3-D model data, usually layer upon layer [1, 2]. With the use of this technology it is possible to fabricate prototypes with minimum material consumption and satisfactory accuracy [3]. Therefore, AM technologies are promising in reducing production costs and time, while maintaining relatively high quality of final products [4] in comparison to traditional manufacturing. Another advantage of this technology is the wide range of materials which can be used

[*] Corresponding author, e-mail: mtychanicz@prz.edu.pl

in production process, including metals, polymers and thermoplastics [1-3]. As far as thermoplastics are concerned, these materials are often applied in fused filament fabrication (FFF) method, which is one of the AM technologies. In the FFF method, thin layers of molten thermoplastic material (filament) are pushed through the movable, heated extrusion nozzle and placed alternately on the print surface to form a final prototype [4-9]. The material used as filament is heated up barely above the melting temperature. The process is fully computer controlled. The FFF is suitable for fabrication of low-cost, piece-production parts due to process simplicity and inexpensive equipment. However, parts fabricated with the use of FFF often suffers from print defects and surface inequality, *e. g.* curvature, warpage, shrinkage [7] *etc.*, which may be caused by inexact adherence of applied layers of material. Consequently, the final part is often non-hermetic and the structure is non-uniform [3, 9, 10]. Therefore, the studies show that mechanical properties of printed components have been investigated in particular [7, 9, 11, 12].

Elements fabricated with the use of 3-D printing technology are mostly applied in medicine, aerospace, automotive, industry, *etc.*, however the new field of application was found in thermal insulation systems, where materials of low thermal conductivity are required (about 0.1 W/mK). It was found that the polylactic acid (PLA) exhibits suitable thermal properties among the materials used in RP technology. The PLA belongs to a group of biopolymers and it is biodegradable aliphatic polyester produced from renewable sources [7, 13, 14]. The PLA has a wide range of applications due to its organic origin and biocompatible properties [3]. In the field of 3-D printing, PLA-based composites are more often applied rather than pure materials.

Although the applicability of this material in thermal protection systems was not especially studied, Trhlikova *et al.* [15] investigated the influence of PLA additives on thermal characteristics of the material. The following thermal parameters were investigated: thermal conductivity, thermal diffusivity, and specific heat. The samples of investigated materials were fabricated using the FFF method. It was found that the thermal conductivity of all samples decreased with time and the additives affected the thermal characteristics.

The application of PLA composite material as thermal insulation in buildings was presented in [16], where the thermal conductivity of PLA-bamboo composite was investigated. In addition the effect of the porosity and the density of material on thermal conductivity was examined. The analysis showed that the average thermal conductivity of the composite was in the range of 0.2 W/mK, what is suitable range in thermal insulation systems.

Morgan *et al.* [17] investigated emissivity of additively manufactured materials using reflectivity meter. The emissivity of common 3-D printing materials such as ABS and PLA reached the average approximate value of 0.92.

According to the remaining properties of PLA, Jonoobi *et al.* [18] investigated mechanical properties of normal and reinforced PLA. The normal PLA tensile modulus was 2.9 GPa, tensile strength was 58.9 MPa, and maximum strain 3.4%.

Drumright *et al.* [19] also studied mechanical properties of PLA. Authors obtained following properties: density 1210 kg/m^3, tensile strength 53 MPa, tensile yield strength 60 MPa, tensile modulus 3.5 GPa, and tensile elongation 2.5-6%. Farah *et al.* [20] collected physical and mechanical properties of PLA. Thermal conductivity in 48 °C was 0.111 W/mK and specific heat in 55 °C was 1590 J/kgK.

The analysis of heat transfer in insulation materials are of great interest due to its complexity, what have been investigated by many authors previously. At elevated temperature the following modes of heat transfer can be distinguished: conduction, radiation, and convection. Each mechanism contributes in different extent to total heat transfer performance, what is sometimes difficult to establish. More detailed information can be found in [21].

This work presents the experimental investigation of thermal conductivity, density, and emissivity of 3-D printed PLA samples. The heat-flow was simulated to identify heat transfer mechanisms (conduction, convection, or radiation) that can occur for specified density. Also the influence of the material orientation on the possibility of free convection was investigated.

Experimental set-up

Thermal conductivity measurement: Measurement of thermal conductivity was conducted on Unitherm 2022 equipment, figs. 1(a) and 1(b). The 2022 model is a fully automated device and it is used for measuring the thermal conductivity of such materials like metals, ceramics, polymers, composites, glass, rubber, and thin specimens like paper products or plastic films. Thermal conductivity is measured according to ASTM E1530 guarded heat-flow meter method.

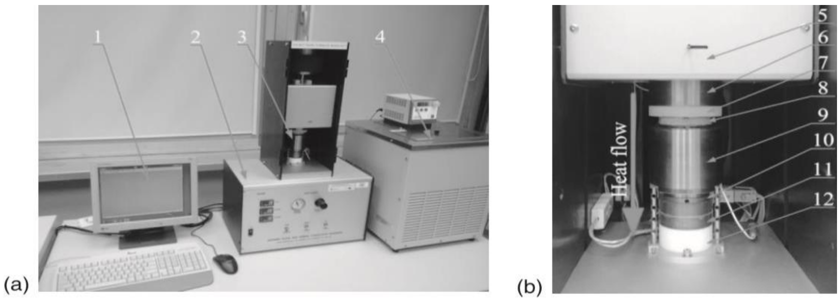

Figure 1. Experimental set-up (a) test section (b); *1 – PC, 2 – controller, 3 – test section, 4 – circulation bath, 5 – guard heater, 6 – top heater, 7 – upper plate, 8 – sample, 9 – lower plate, 10 – reference calorimeter, 11 – bottom heater, 12 – heat sink*

The test section is presented in fig. 1(b). A sample of the investigated material is held under a reproducible compressive load between two polished metal surfaces, each controlled at a different temperature. The lower contact surface is a part of a calibrated heat flux sensor. As heat-flows from the upper surface through the sample to the lower surface, an axial temperature gradient is established in the stack. By measuring the temperature difference across the sample (between the upper and the lower plate surfaces in contact with the specimen) along with the output from the heat flux meter, thermal conductivity of the sample can be determined when its thickness is known. Unitherm 2022 is used to measure the thermal conductivity in the range of 0.1-40 W/mK and in the temperature range of 10-300 °C. The sample of the tested material has a shape of a cylinder with an external diameter of 50.8 mm and a height depending on the expected thermal conductivity and the better insulating properties of the material, the minor thickness of the material. In order to minimize thermal contact resistance, thermal grease is applied on the surface of the plates. For each sample three measurements of thermal conductivity were made. Each measurement was carried out after dismantling and re-mounting of the sample in the test section. The thermal conductivity was performed for the sample average temperature T = 40 °C and a temperature drop on the sample was ΔT = 50 °C. The pressure exerted on the sample was about 172 kPa. Uncertainity of the thermal conductivity measurement was 8.4% [22]. The laboratory room, in which the measurements were conducted, was air conditioned and a constant temperature and relative humidity of 20 °C and 50%, respectively, were maintained.

Density measurement PLA density measurements were made by measuring the mass and volume of the investigated sample. Mass measurements were made by using the RADWAG XA 210/Y balance with a resolution of 0.01 mg and a maximum measuring range of 210 g. Volumetric measurements were made by measuring the diameter and height of the sample with the use of a micrometer with 0.01 mm resolution. The samples are non-isotropic, therefore measured density should be treated as an average value. Density measurement was carried out at ambient temperature. Uncertainity of the density measurement was 1.1% [22].

Emissivity measurement PLA emissivity measurements were made by printing the flat round PLA sample with 0.2 mm thickness and diameter of 100 mm. The sample was attached to the flat electric heater and the surface temperature was measured with calibrated contact thermometer (small flat thermocouple). The sample surface emissivity was estimated by infrared camera FLIR P640 with the spectral range of the detector 8-14 μm. The emissivity of blue PLA was $\varepsilon = 0.96$.

Samples Samples were designed in CAM program and next prepared by FFF RP method. The Wanhao Duplicator i3 3-D printer with MK10 single-head extruder was used for the production of samples. The working area of the device is 200 × 200 × 180 mm. Nine samples with variable internal air cells were fabricated. Each sample had the shape of a disk with an outer diameter of $d = 50.8$ mm and a total height of $t = 10$ mm (figs. 2 and 3.). The accuracy of the sample geometrical dimensions was better than ±0.4 mm.

The samples were closed by external surfaces. Inside each sample there were perpendicular walls forming cuboidal air cells. Each air cell had the same height of 8.4 mm but different base dimensions, for example sample 8 × 8 had air cell with dimensions 8 × 8 × 8.4 mm. Additionally, the solid sample and empty sample were tested. The empty sample had only external walls. Both walls (internal and external) had the thickness of 0.8 mm, fig. 3. With the change of the cell size, the average density of the sample varied from $\rho = 273$ kg/m for empty sample to $\rho = 1150$ kg/m for the solid one. The technological parameters of the RP method were: the temperature of the nozzle was 195 °C, the temperature of the bed was 50 °C, the filament diameter was 1.75 mm, the layer thickness was set at 0.2 mm, and the printing speed was 15 mm/s. The time of printing of 8 × 8 sample was about one hour, while the solid sample was printed about five hours.

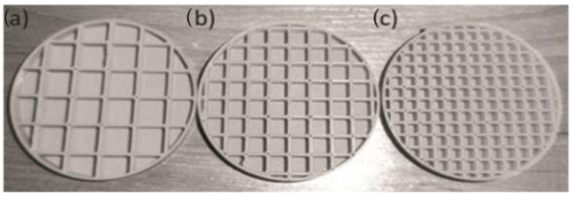

Figure 2. Cross-section of PLA samples with different cell: (a) 8 × 8, (b) 5 × 5, (c) 3 × 3

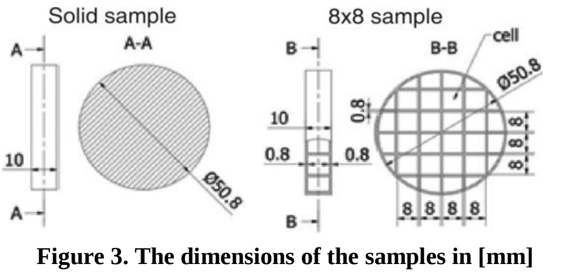

Figure 3. The dimensions of the samples in [mm]

Numerical modeling

Numerical simulation has been used to investigate heat transfer mechanism in the tested materials. In the present case, combined process of heat conduction in solid body, surface radiation, and natural convection in air cavity was determined using commercial software COMSOL Multiphysics version 5.2. The computational domain included single hexahedral cell, see fig. 4 (a). The sample consisted of the air-filled cavity and the solid body. The four external vertical walls of the computational domain are perfectly insulated, while the two horizontal walls (upper and lower) are maintained at two different temperatures T_h and T_c, respectively, where $T_h > T_c$, see fig. 4 (b). It was assumed that the problem is 3-D and steady-state. The air-filled cavity is incompressible, energy dissipation function is negligible and there are no internal heat sources. All of the solid body and fluid properties remained constant at average temperature, T_0, except for the density of the air, whose variation with the temperature is allowed in the buoyancy term. In addition, the temperature difference in the flow domain is small enough to justify the use of the Boussinesq approximation. Thus, buoyancy effects are studied due to the gravity effect. The inner surfaces, in contact with the air, are assumed to be gray and diffuse and they transfer heat via radiation. The emissivity of the internal walls in the enclosure is held constant and the absorptivity is equal to the emissivity by Kirchoff's law.

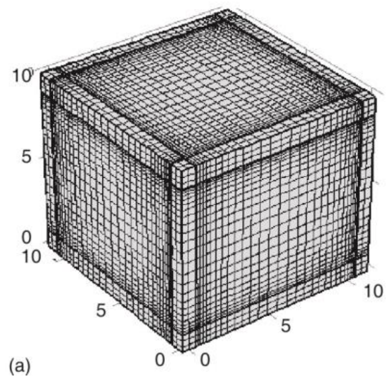

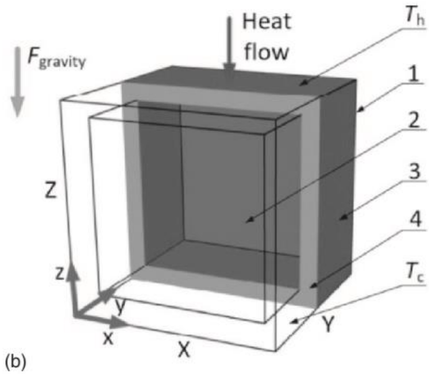

Figure 4. The cell mesh (a), co-ordinate system (b); *1 – cell surface, 2 – air inside cell, 3 – adiabatic wall, 4 – PLA sample*

The governing equations are:

– continuity equation for a 3-D steady incompressible flow:

$$\frac{\partial u}{\partial x}+\frac{\partial v}{\partial y}+\frac{\partial w}{\partial y}=0 \tag{1}$$

– momentum equation for 3-D steady laminar, incompressible flow:

$$\rho_0\left(u\frac{\partial u}{\partial x}+v\frac{\partial u}{\partial y}+w\frac{\partial u}{\partial z}\right)=f_x-\frac{\partial p}{\partial x}+\mu_0\left(\frac{\partial^2 u}{\partial x^2}+\frac{\partial^2 u}{\partial y^2}+\frac{\partial^2 u}{\partial z^2}\right)$$

$$\rho_0\left(u\frac{\partial v}{\partial x}+v\frac{\partial v}{\partial y}+w\frac{\partial v}{\partial z}\right)=f_y-\frac{\partial p}{\partial y}+\mu_0\left(\frac{\partial^2 v}{\partial x^2}+\frac{\partial^2 v}{\partial y^2}+\frac{\partial^2 v}{\partial z^2}\right) \tag{2}$$

$$\rho_0\left(u\frac{\partial w}{\partial x}+v\frac{\partial w}{\partial y}+w\frac{\partial w}{\partial z}\right)=f_z-\frac{\partial p}{\partial z}+\mu_0\left(\frac{\partial^2 w}{\partial x^2}+\frac{\partial^2 w}{\partial y^2}+\frac{\partial^2 w}{\partial z^2}\right)$$

The buoyancy force was modeled by using Boussinesq approximation [23]:

$$f=-\rho_0\frac{T-T_0}{T_0}g \tag{3}$$

where

$$T_0=\frac{T_h+T_c}{2} \tag{4}$$

Energy equation for fluid:

$$\rho_0 c_0\left(u\frac{\partial T}{\partial x}+v\frac{\partial T}{\partial y}+w\frac{\partial T}{\partial z}\right)=k_0\left(\frac{\partial^2 T}{\partial x^2}+\frac{\partial^2 T}{\partial y^2}+\frac{\partial^2 T}{\partial z^2}\right) \tag{5}$$

Energy equation for solid:

$$\frac{\partial^2 T_s}{\partial x^2}+\frac{\partial^2 T_s}{\partial y^2}+\frac{\partial^2 T_s}{\partial z^2}=0 \tag{6}$$

On the basis of energy balance and Fourier law for solid-fluid interface, the heat flux density can be described:

$$k_0\frac{\partial T}{\partial n}=k_s\frac{\partial T_s}{\partial n} \tag{7}$$

where n denotes the normal direction to the surface, k_0 [Wm^{-1}K^{-1}] – the air thermal conductivity, k_s [Wm^{-1}K^{-1}] – the PLA thermal conductivity.

The determination of the radiative flux requires the knowledge of the surface temperature. The equation of the thermal balance of each surface provides to these temperatures. Thus, the assumption that the solid surfaces are in thermal equilibrium, leads to equation:

$$-k_0\frac{\partial T}{\partial n}+q_R=0 \tag{8}$$

where q_R [Wm^{-2}] is the net radiative flux density.

The net radiative flux for a diffuse-gray and opaque internal cavity surface A_i can be expressed:

$$A_i q_{Ri}=A_i(J_i-G_i)=A_i\left(J_i-\sum_j F_{ij}J_j\right) \tag{9}$$

$$A_i q_{Ri}=A_i\varepsilon_i\left(E_{bi}-\sum_j G_j\right)=A_i\varepsilon_i\left(E_{bi}-\sum_j F_{ij}J_j\right) \tag{10}$$

where J_i is the radiosity of the surface A_i , F_{ij} – the view factor, and E_{bi} – the blackbody radiation.

Combining (9) it is possible to determine the radiosity J_i from equation:

$$J_i-(1-\varepsilon_i)\sum_j F_{ij}J_j=\varepsilon_i E_{bi} \tag{11}$$

and then the net radiative flux density q_R from eq. (9).

Mesh geometry The computational domain was meshed by hexahedral, quadrilateral, edge and vertex elements with smooth transition to avoid rapid changes in mesh density. To attain the grid independency, the effective thermal conductivity was tested with ΔT = 50 °C, T_0 = 40 °C for different mesh sizes. The results are listed in tab. 1. It was found that the variation of the effective thermal conductivity among all mesh sizes was not significant.

Table 1. The effective thermal conductivity for different mesh sizes

ρ [kgm^{-3}]	Cell size [mm]	t [mm]	No. of elements	k_e [Wm^{-1}K^{-1}]
192	200 × 200	10	12544	0.095
222	40 × 40	10	6400	0.099
322	10 × 10	10	6480	0.114
192	200 × 200	10	14400	0.095
222	40 × 40	10	11520	0.099
322	10 × 10	10	8800	0.114
192	200 × 200	10	23120	0.095
222	40 × 40	10	14872	0.098
322	10 × 10	10	14976	0.114

Boundary conditions Numerical simulation was carried out in steady-state conditions. The air was the working fluid inside the cell. Boundary conditions are presented in fig. 4(b). The upper isothermal wall with higher temperature T_h = idem and lower isothermal wall at a lower temperature T_c = idem was assumed in order to enforce the heat-flow.

An adiabatic condition on the other external walls was assumed:

$$\frac{\partial T}{\partial x} = \frac{\partial T}{\partial y} = 0 \tag{12}$$

Also no-slip condtion was assumed at all internal surfaces of the cavity:

$$u = v = w = 0 \tag{13}$$

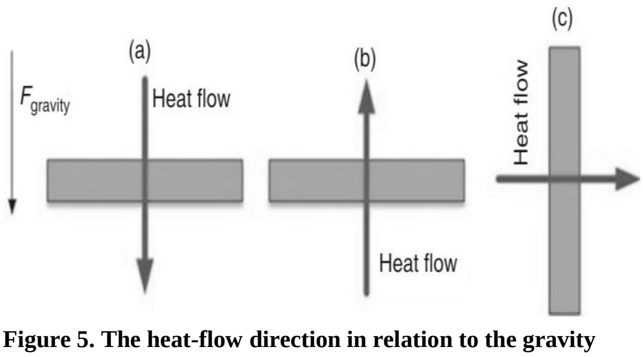

Figure 5. The heat-flow direction in relation to the gravity force; (a) heat-flow down, (b) heat-flow up, and (c) heat-flow to the side

All of the internal surfaces exchanged heat by radiation. Due to the free convection that can occur inside the cell, the influence of the gravity force was studied. The direction of the heat-flow has been taken once in line, opposite and transversely to the gravity force, sees fig. 5.

Experimental results

The results of experimental investigations of the effective thermal conductivity, emissivity and density are presented in this section. Figure 6(a) shows the average sample density for different cell dimensions. The density of solid material was ρ = 1150 kg/m^3, while for *empty* sample the density was ρ = 237 kg/m^3. By using the RP method it is possible to reduce the density by almost five times with respect to the solid material, see fig. 6(a). The *empty* sample, except low density, is characterized by high susceptibility to destruction, even under low pressure load due to the lack of ribs inside the material.

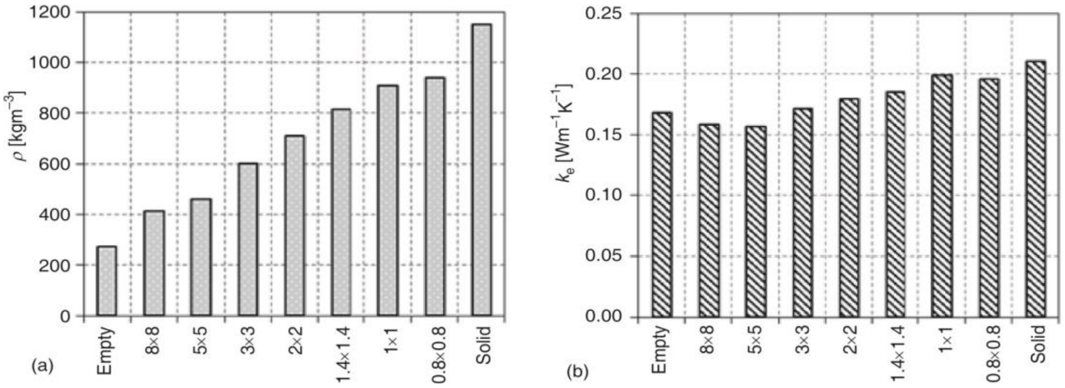

Figure 6. The average density (a) effective thermal conductivity (b) of the investigated samples

Figure 6(b) shows the effective thermal conductivity, k_e, for different cell dimensions. The highest value of effective thermal conductivity was denoted for solid material k_{solid} = 0.22 W/mK. With density reduction, the thermal conductivity decreased, reaching a local minimum for 5 × 5 cell, where the thermal conductivity is about 30% less than for the solid material (k_e = 0.153 W/mK). For samples of smaller cell dimensions, the effective thermal conductivity is stabilized at approximate value $k_e \approx$ 0.16 W/mK. Figure 7 (a) presents the comparison of thermal conductivity of typical polymer materials at ambient temperature. The PLA has thermal conductivity similar to such materials like: PVC, PMMA, and PP. The relatively low value of thermal conductivity allows qualifying PLA to the group of insulating materials.

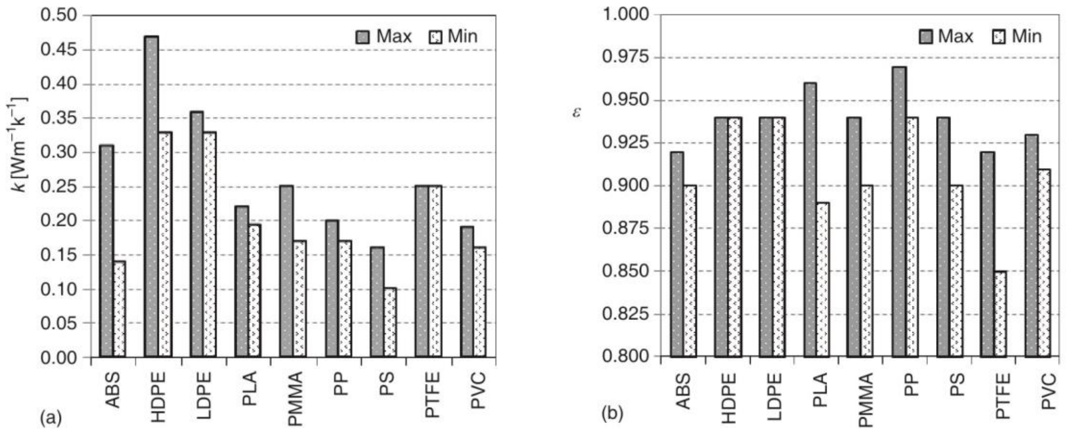

Figure 7. Comparison of typical thermal conductivity (a) [24-26] and average emissivity (b) [27] of common polimers in ambient temperature

The emissivity of typical plastics is presented in fig. 7(b). It can be seen that major polymer-based materials have similar emissivity of about 0.9. The measured emissivity of blue PLA was 0.96.

Numerical results

A comparison of the effective thermal conductivity for different heat-flow directions is presented in fig. 8(a). As can be seen, there are negligibly small differences between effective thermal conductivity for different heat-flow directions, except the area: $200 < \rho < 400$ kg/m^3. It means that the influence of the heat-flow direction has negligible effect on effective thermal conductivity. Furthermore, the results of experimental measurements and numerical simulations of the effective thermal conductivity for down heat-flow direction are convergent.

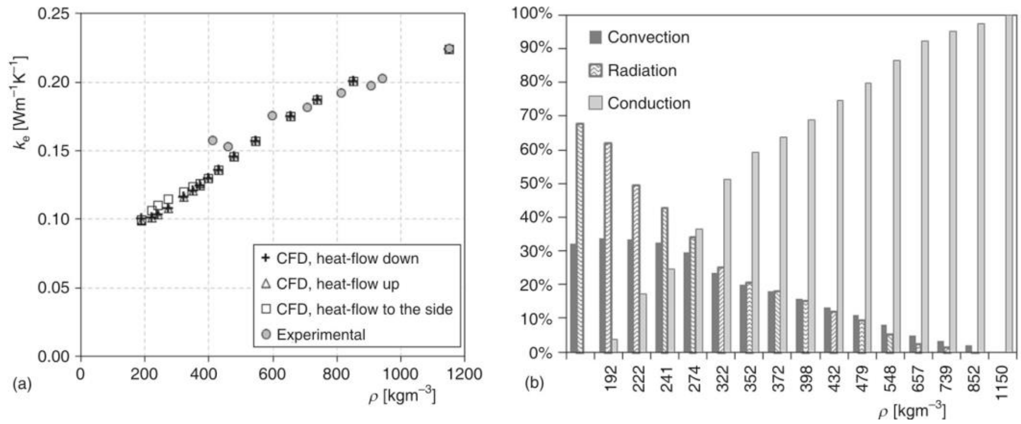

Figure 8. The comparison of effective thermal conductivity of PLA samples (a), the part of heat transfer mechanism in effective heat conduction for heat-flow to the side (b)

In this case convection, conduction, and radiation play significant role in heat transfer and effective thermal conductivity of PLA depends on these heat transfer modes. Therefore, fig. 8(b) shows the percentage contribution of each heat transfer mode. As can be seen, with density decrease, the contribution of heat conduction drops significantly, while the convection and radiation increase. Due to high emissivity of PLA, the impact of radiative heat transfer on the effective thermal conductivity is significant, particularly for small densities.

In turn, fig. 9 presents the influence of heat transfer mechanism on thermal conductivity ratio k_e/k_{solid}. In order to reduce radiant heat transfer in the cavity, highly reflective coatings can be used. In this way, an insulating material with a relatively low effective thermal conductivity can be obtained. Figures 10-12 present the general outline of the flow for different cell height to width ratio, *i. e*. aspect ratio of the cells. For high value of the aspect ratio, fig. 10, the flow increases in magnitude near the center of the upper and lower wall. The zone

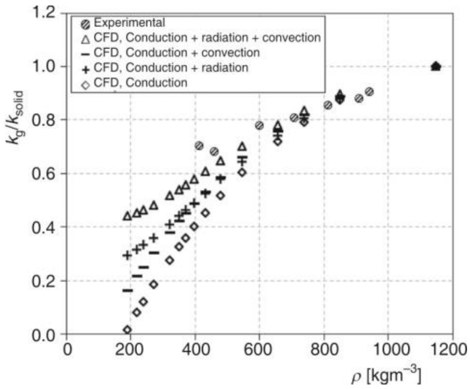

Figure 9. The comparison of thermal conductivity ratio k_e/k_{solid}-heat-flow down

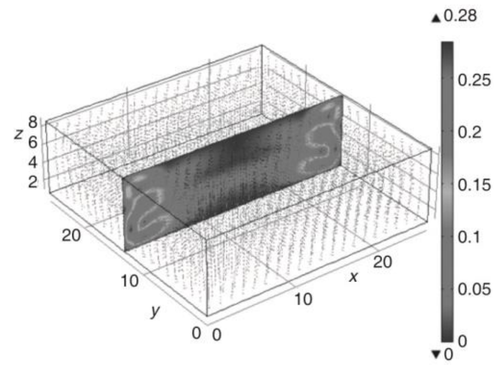

Figure 10. Velocity field inside the cell, heat-flow down, value in [mms^{-1}]

of velocity magnitude increase shifts to the center of the cell at lower aspect ratio, fig. 11. In turn, for low aspect ratio, fig. 12, the flow increases near the corners of the cell.

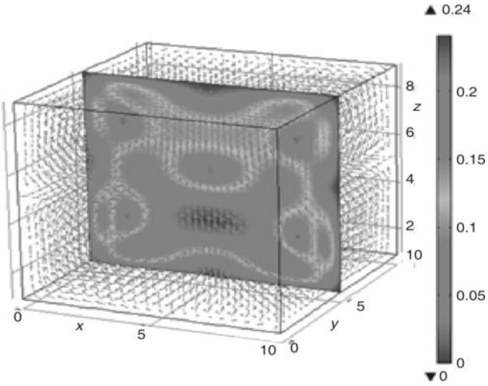

Figure 11. Velocity field inside the cell, heat-flow down, value in [mms^{-1}]

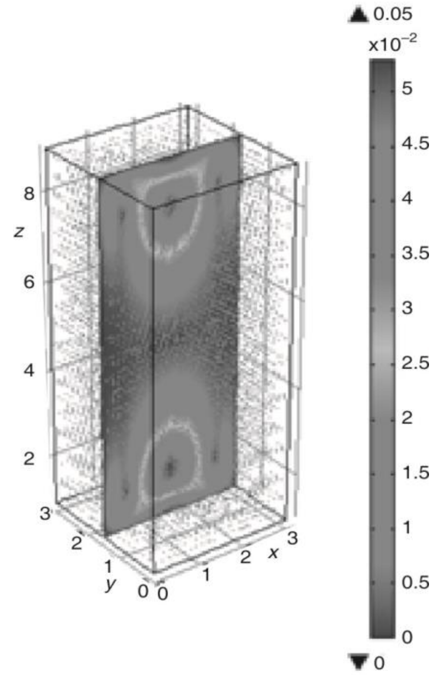

Figure 12. Velocity field inside the cell, heat-flow down, value in [mms^{-1}]

Conclusion

This work presents the experimental results of the effective thermal conductivity of PLA and numerical investigation of combined process of heat conduction in solid body, surface radiation, and natural convection. Validation of the numerical results was made on the basis of experimental investigation of the effective thermal conductivity. The predicted effective thermal conductivity of the PLA from the numerical simulations was compared with the experimental results. A satisfactory agreement between the experimental and numerical results was achieved. A numerical study of combined laminar natural convection, conduction and surface radiation heat transfer in a cavity showed that the convection and radiation heat losses played significant role in heat transfer performance. The results of the simulation showed that the radiative heat transfer contribution along the surfaces is the dominant heat transfer mode for low density of the sample. In addition, the effect of the sample orientation on heat transfer in a cavity was also investigated. The heat-flow direction does not significantly affect the effective thermal conductivity.

Nomenclature

c_0 – air specific heat, [Jkg^{-1}K^{-1}]
d – diameter, [m]
g – acceleration of gravity, [ms^{-2}]
k – thermal conductivity, [Wm^{-1}K^{-1}]
k_e – effective thermal conductivity, [Wm^{-1}K^{-1}]
k_{solid} – solid thermal conductivity [Wm^{-1}K^{-1}]
t – height, [m]
T – sample average temperature, [°C]
ΔT – temperature drop on the sample, [°C]
T_c – temperature of the lower isothermal wall, [°C]
T_h – temperature of the upper isothermal wall, [°C]
T_0 – average temperature, [°C]

Greek symbols

ε – emissivity, [–]
ρ – density, [kgm^{-3}]

Subscripts

s – solid
o – fluid

Acronyms

ABS – acrylonitrile butadiene styrene
AM – additive manufacturing
FFF – fused filament fabrication
HDPR – high-density polyethylene
LDPE – low-density polyethylene
PLA – polylactic acid
PMMA – polymethyl methacrylate
PP – polypropylene
PS – polystyrene
PTFE – polytetrafluoroethylene
PVC – polyvinyl chloride
RP – rapid prototyping

References

[1] ***, ASTM F2792-12a, Standard Terminology for Additive Manufacturing Technologies' (Withdrawn 2015), ASTM International, West Conshohocken, Penn., USA, 2012
[2] Kumar, S., Kruth, J.-P., Composites by Rapid Prototyping Technology, *Materials and Design*, *31* (2010), 2, pp. 850-856
[3] Wang, X., *et al*., 3D Printing of Polymer Matrix Composites: A Review and Prospective, *Composites Part B*, *110* (2017), Feb., pp.442-458
[4] Matta, A. K., *et al*., The Integration of CAD/CAM and Rapid Prototyping in Product Development: A review, *Materials Today: Proceedings*, *2* (2015), 4-5, pp. 3438-3445
[5] Melnikova, R., *et al*., 3D Printing of Textile-Based Structures by Fused Deposition Modelling (FDM) with Different Polymer Materials, *IOP Conference Series: Materials Science and Engineering*, *62* (2014), 1, 012018
[6] Tran, P., *et al*., Bimaterial 3D Printing and Numerical Analysis of Bio-Inspired Composite Structures Under In-Plane and Transverse Loadings, *Composite Part B*, *108* (2017), Jan., pp. 210-223
[7] Murariu, M., Dubois, P., PLA Composites: From Production to Properties, *Advanced Drug Delivery Reviews*, *107* (2016), Dec., pp. 17-46
[8] Rayna, T., Striukova, L., From Rapid Prototyping to Home Fabricatrion: How 3D Printing is Changing Business Model Innovation, *Technological Forecasting & Social Change, 102* (2016), Jan., pp. 214-224
[9] Kochesfahni, Saied, H., Improving PLA-Based Material for FDM 3D-Printers Using Minerals (Principles and Method Development), *Proceedings*, 2016 SPE ANTEC Conference, Indianapolis, Ind., USA, 2016, pp. 1598-1614
[10] Gajdoš, I., Slota, J., Influence of Printing Conditions on Structure in FDM Prototypes, *Technical Gazette*, *20* (2013), 2, pp. 231-236
[11] Drummer, D., *et al*., Suitability of PLA/TCP for Fused Deposition Modeling, *Rapid Prototyping Journal*, *18* (2012), 6, pp. 500-507
[12] Tymrak, B. M., *et al*., Mechanical Properties of Components Fabricated with Open-Source 3-D Printers Under Realistic Environmental Conditions, *Materials and Design*, *58* (2014), Jun, pp. 242-246
[13] Pretula, J., *et al*., Polylactides- Methods of Synthesis and Characterization, *Advanced Drug Delivery Reviews*, *107* (2016), Dec., pp. 3-16
[14] Lebedov, S. M., *et al*., Poly(Lactic Acid)-Based Polymer Composites with High Electric and Thermal Conductivity and their Charazterization, *Polymer Testing*, *58* (2017), Apr., pp. 241-248
[15] Trhlikova, L., *et al*., Study of the Thermal Properties of Filaments for 3D Printing, *AIP Conference Proceedings*, *1752* (2016), 1, 040027
[16] Kusano, K., *et al*., Thermal Characteristics of PLA-Bamboo Composites, *High Performance Structures and Materials IV*, *97* (2008), Apr., pp. 175-183
[17] Morgan, R. V., *et al*., Emissivity Measurements of Additively Manufactured Materials, LA-UR-17-20513 Report, Los Almos, N. Mex., USA, 2017
[18] Jonoobi, M., *et al*., Mechanical Properties of Cellulose Nanofiber (CNF) Reinforced Polylactic Acid (PLA) Prepared by Twin Screw Extrusion. *Composites Science and Technology*, *70* (2010), 12, pp. 1742-1747
[19] Drumright, R. E., *et al*., Polylactic Acid Technology. *Advanced materials*, *12* (2000), 23, pp. 1841-1846
[20] Farah, S., *et al*., Physical and Mechanical Properties of PLA, and their Functions in Widespread Applications—A Comprehensive Review. *Advanced Drug Delivery Reviews*, *107* (2016) Dec., pp. 367-392
[21] Tychanicz-Kwiecien, M., *et al*., Review of High-Temperature Thermal Insulation Materials, *Journal of Thermophysics and Heat Transfer*, *33* (2019), 1, pp. 271-284

[22] ***, ISO/IEC Guide 98-3:2008(en) Uncertainty of Measurement- Part 3: Guide to the Expression of Uncertainty in Measurement (GUM:1995)
[23] Wilcox, D. C., *Turbulence Modeling for CFD*, DCW industries, Inc., Glendale, Cal., USA, 1993
[24] Lienhard, IV, J. H., Lienhard V, J. H., *A Heat Transfer Textbook*. Phlogiston Press, Cambridge, Mass., USA, 2001
[25] Hussain, A. R. J., *et al*., Review of Polymers for Heat Exchanger Applications: Factors Concerning Thermal Conductivity, *Applied Thermal Engineering*, *113* (2017), Feb., pp. 1118-1127
[26] Choy, C. L., Thermal Conductivity of Polymers, *Polymer*, *18* (1977), 10, pp. 984-1004
[27] ***, TESTO, Pocket Guide Thermography. Theory – Practical Application – Tips & Tricks, Testo SE & Co. KGaA, 2017

Paper submitted: September 17, 2018
Paper revised: October 20, 2018
Paper accepted: January 24, 2019